

17 Simultaneous Acquisition of Multiple Forms of fMRI Contrast

E.C. WONG, P.A. BANDETTINI

CONTENTS

17.1	Rationales for Embedded Techniques	183
17.2	TE Stepping	184
17.3	Combined Gradient-Echo, Spin-Echo and Asymmetric Spin-Echo Acquisitions	184
17.3.1	Gradient Echoes with Spin-Echoes	184
17.3.2	Gradient Echoes with Asymmetric Spin-Echoes	185
17.4	Simultaneous BOLD and Perfusion fMRI	186
17.4.1	Imaging Techniques	187
17.4.2	Separation of BOLD and Perfusion Signals in Pulsed ASL	188
17.5	Embedded Diffusion Weighting	189
17.6	Conclusions	190
	References	191

17.1 Rationales for Embedded Techniques

Functional MRI is a rapidly growing technique for the assessment of neuronal activation locations, timings, and magnitudes. It is also becoming a useful tool for the characterization of cerebral physiology in general. As discussed in several other chapters in this volume, several different types of physiologic information can be mapped using fMRI. These include baseline cerebral blood volume (CBV) (ROSEN et al. 1989; MOONEN et al. 1990); changes in blood volume (BELLIVEAU et al. 1991); baseline and changes in cerebral perfusion (WILLIAMS 1992; DETRE 1992; EDELMAN 1994; KWONG 1994; WONG 1997; WONG 1998; KIM 1995); changes in blood oxygenation (OGAWA et al. 1990; TURNER et al. 1991; KWONG et al. 1992; OGAWA and LEE 1992; BANDETTINI et al. 1992; FRAHM et al. 1992; HAACKE

et al. 1997); and changes in $CMRO_2$ (DAVIS 1998; KIM and UGURBIL et al. 1997; VANZIIL et al. 1998).

Several studies have involved the comparison – using activations or physiologic stresses – of the locations, timings, and magnitudes of fMRI signal changes across different contrast weightings. Information from two or more contrast weightings is extremely helpful in the study of fMRI contrast mechanisms. For example, the ratio of spin-echo to gradient-echo signal changes may reveal the predominant susceptibility perturber size. The dynamics of cerebral blood flow (CBF) changes relative to BOLD changes may reveal details of the underlying changes in CBV and $CMRO_2$.

Comparisons across pulse sequence weightings are typically made by performing separate experiments (collecting separate sets of time series data) for each pulse sequence or test used. The utility of these comparisons is directly related to how accurately they can be made. Hindrances to accurate comparison of these changes include subject motion between separate time series, activation or hemodynamic change non-repeatability (due to changing cognitive or hemodynamic state over time) within and across separate time series, and system instabilities. Simultaneous collection of different contrast weightings is a solution to these problems. We will refer to this type of strategy as “embedded” contrast weighting, since two or more types of contrast are embedded in a single time series or following a single excitation.

Types of embedded contrast include nearly limitless combinations of the following: (a) TE stepping in a single time series to obtain data on T_2^* (or T_2) and S_0 (the extrapolated signal at $TE=0$), (b) multiple echoes in a single excitation, (c) gradient-echoes, spin-echoes, and asymmetric spin-echoes, (d) diffusion weighting, (e) arterial spin labeling (ASL) for measurement of CBF, and (f) magnetization transfer contrast. Several combinations of these types of contrast are described in more detail below.

E.C. WONG, PhD, MD; Departments of Radiology and Psychiatry, University of California at San Diego Medical Center, 200 West Arbor Drive, San Diego, CA 92103-8756, USA
P.A. BANDETTINI, PhD; Biophysics Research Institute, Medical College of Wisconsin, 8701 Watertown Plank Rd., Milwaukee, WI 53226, USA

17.2 TE Stepping

Assuming that a gradient-echo sequence is used, the resting and activated MRI signal, S_r and S_a , respectively, can be approximated by:

$$\begin{aligned} S_r &= S_{r0} e^{-R_2^* r TE} \\ S_a &= S_{a0} e^{-R_2^* a TE} \end{aligned} \quad (17.1)$$

The resting and activated signals at TE=0 (S_{r0} and S_{a0}), are modulated by changes in proton density, T_1 , or inflow. Transverse relaxation rates, $R_2^* r$ ($1/T_2^* r$) and $R_2^* a$ ($1/T_2^* a$) are modulated by changes in the magnetic susceptibility. If TE is systematically modulated during a time series collection of data, temporally and spatially registered measurements of R_2^* and S_0 during rest and activation are possible, allowing separation of inflow (non-susceptibility) and oxygenation (susceptibility) effects.

An example of this technique is shown in Figs. 17.1 and 17.2, in which a time series of echo planar images was acquired. The TE was stepped between each image; five cycles were acquired. In these data, it appears that a change in S_0 and T_2^* takes place in the motor cortex during finger tapping.

Reports describing several different manifestations of TE stepping have appeared in the literature, including multi-echo high-resolution measurements at 4T (MENON et al. 1993), multi-echo low spatial resolution high echo time resolution EPI readout techniques (POSSE et al. 1995 1997; BANDETTINI and WONG 1998a), ; spectroscopic techniques for separating out inflow and susceptibility-related causes for the rapidly occurring pre-undershoot (HENNIG et al. 1994, 1995); double-echo spiral scan (GLOVER

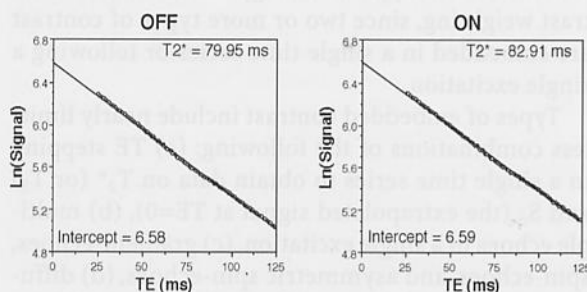


Fig. 17.1. TE dependence of the resting and activated gradient-echo signal. Each point on the decay curve is an average of five echo planar images acquired during a single time series. TR=500 ms. A change in the intercept is likely due to a change in inflow. A change in the slope (R_2^*) is due to changes in oxygenation and/or blood volume

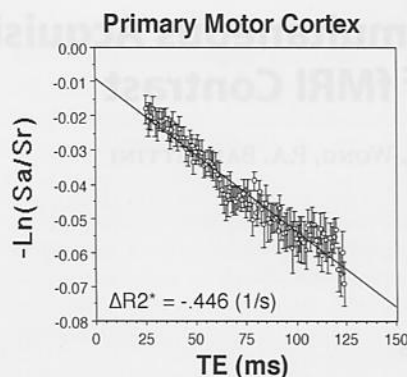


Fig. 17.2. Plot combining the two curves shown in Fig. 17.1

et al. 1996), and single-echo EPI time series, in which the TE was incremented with each successive image (BANDETTINI et al. 1994, 1997).

In addition to the study of contrast mechanisms, the acquisition of two or more gradient echoes allows for B_0 field mapping at every time point. Real time B_0 field mapping may allow correction for dynamic artifacts caused by speaking, swallowing, and breathing (BIRN et al. 1997a,b).

17.3 Combined Gradient-Echo, Spin-Echo, and Asymmetric Spin-Echo Acquisitions

17.3.1 Gradient Echoes with Spin-Echoes

In general, the activation-induced signal changes in spin-echo sequences are thought to arise primarily from blood oxygenation-related field perturbations around red blood cells and capillaries (small compartments). The changes in gradient-echo sequences are thought to arise from field perturbations around red blood cells, capillaries, and larger vessels as well (compartments of all sizes). The ratio of these signal changes, with activation or with the administration of exogenous contrast, may give specific information about the predominant compartment size in each voxel – leading to greater certainty of activation foci (WEISKOFF et al. 1994; OGAWA et al. 1993; BANDETTINI and WONG 1995; KENNAN et al. 1994). Voxel-wise comparisons of these changes require precise registration. A method for precise registration involves the collection of a gradient-echo image, then application of a 180° pulse and subse-

Combined Gradient - Echo and Spin - Echo EPI

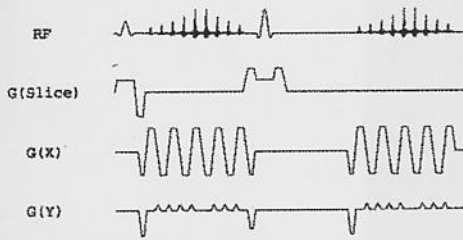


Fig. 17.3. Combined gradient-echo and spin-echo echo planar imaging (EPI), allowing for the collection of spin-echo (T_2 -weighted) echo planar image pairs within about 50 ms of each other. This sequence is used to obtain spatially and temporally registered gradient-echo and spin-echo time course series for voxel-wise comparison of activation-induced signal change dynamics with different contrast weightings

quent collection of a spin-echo image (BANDETTINI et al. 1993, 1994; BANDETTINI and WONG 1998b; BANDETTINI 1995; PRINSTER 1997). This approach to image acquisition substantially reduces the small amount of systematic error that occurs across separate trials. The pulse sequence is shown in Fig. 17.3.

Typical time series collected using this acquisition strategy are shown in Fig. 17.4. Both time series are from identical voxels in motor cortex. Figure 17.4a is during administration of a bolus of gadolinium during rest. Figure 17.4b is during cyclic on-off finger tapping. Figure 17.5 shows a type of comparison possible with this technique. Changes in R_2^* and R_2 , induced by a bolus injection of gadolinium, are compared on a voxel-wise basis.

Image pairs and BOLD contrast functional images created from combined gradient-echo and spin-echo time series are shown in Fig. 17.6. Lastly, systematic incrementation of the two TE values in each sequential time course image also enables the simultaneous mapping of relative transverse relaxation rates (R_2^* , R_2 , and R_2') and longitudinal magnetizations (S_0), as well as changes in these values, as shown in Figs. 17.7 and 17.8. Using this method of analysis, a decrease in R_2 is minimally perceptible, and S_0 changes are relatively imperceptible. The reason for this last observation may be that the TR was suboptimal for detection of S_0 changes or that the susceptibility-induced transverse relaxation rate changes do not behave as single exponential functions.

17.3.2

Gradient Echoes with Asymmetric Spin-Echoes

In a variation on the theme described above, one or two asymmetric spin-echoes can be acquired instead of the spin-echo. If the echo planar imaging (EPI) readout window is sufficiently short, then three equally T_2' -weighted images can be obtained within ~ 150 ms, each having a different T_2 weighting. The first image is collected during the FID, the second prior to the spin-echo (offset by $-\tau$), and the third after the spin-echo (offset by $+\tau$).

Figures 17.9 and 17.10 show an example of this strategy. A time series of 200 axial image triplets was collected: in-plane voxel dimension= 3.8×3.8 mm, slice thickness= 7 mm, TR= 1 ms, gradient echo TE= 27.1 ms. The spin-echo occurred at 109.6 ms, and two asymmetric spin-echoes were collected at t offsets of ± 27.1 ms. During collection of the time series, self-paced bilateral finger tapping was performed in a cyclic manner (20 s on/20 s off). Figure 17.9 shows the first anatomical images (TR= 8) and functional images obtained using this technique. Figure 17.10 shows time series from the same voxels in the motor cortex. Because of T_2 decay, the signal-to-noise ratio in each image decreases, and correspondingly, the contrast-to-noise ratio in the functional images decreases. The functional contrast-to-

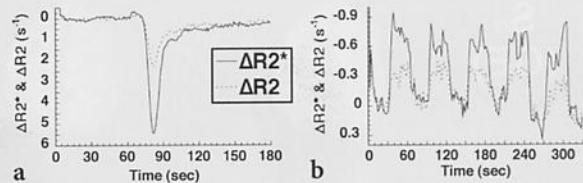


Fig. 17.4a,b. ΔR_2^* and ΔR_2 from identical regions during a bolus injection of a susceptibility contrast agent and b brain activation. A combined gradient-echo and spin-echo sequence were used

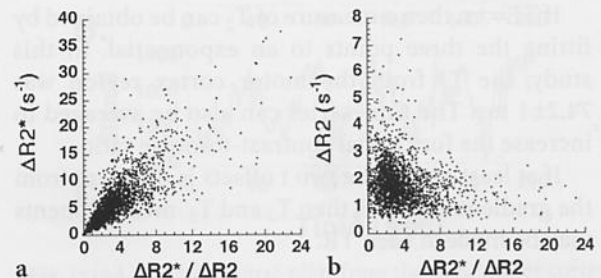


Fig. 17.5a,b. Plots from gray matter of BOLD $\Delta R_2^*/\Delta R_2$ vs a ΔR_2^* and b ΔR_2 . Significantly different correlations are seen

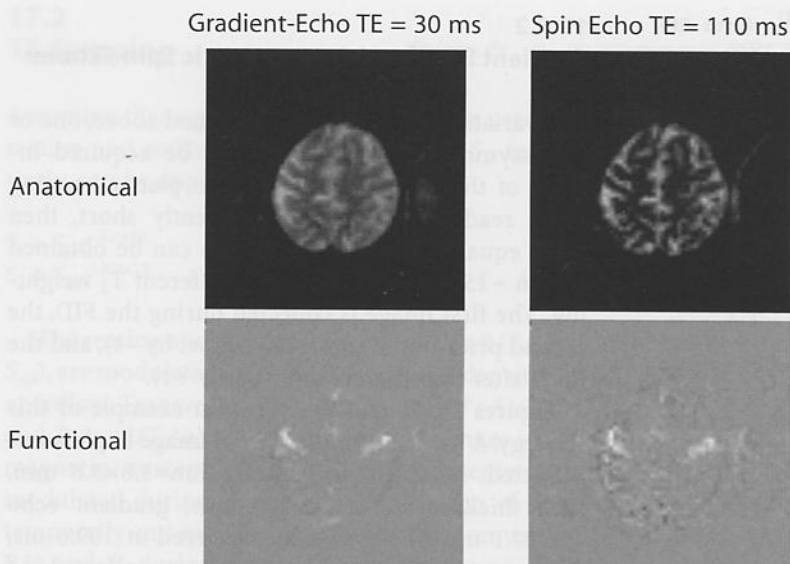


Fig. 17.6. A pair of anatomical images and the corresponding functional correlation images obtained simultaneously from combined gradient-echo and spin-echo time course series

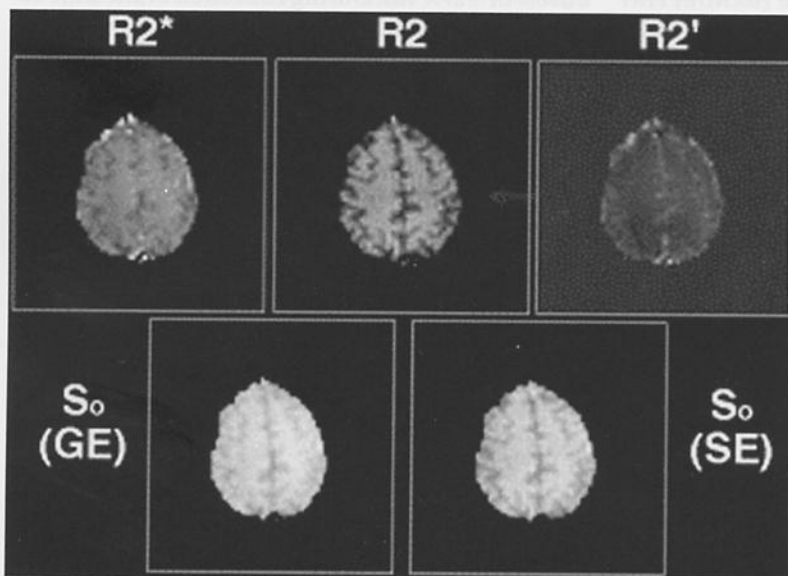


Fig. 17.7. Resting state transverse relaxation rate and S_0 images. The R_2' image ($=R_2^* - R_2$) is a direct indicator of proton resonance line width

noise ratios in the same motor cortex region were 4.9, 2.0, and 1.6 for the three functional data sets, respectively.

If $TE = \pm\tau$, then a measure of T_2 can be obtained by fitting the three points to an exponential. In this study, the T_2 from the motor cortex region was 74.2 ± 1 ms. The time series can also be averaged to increase the functional contrast-to-noise ratio.

If at least one of the two t offsets is different from the gradient-echo TE, then T_2 and T_2' measurements may be made at each TR.

17.4 Simultaneous BOLD and Perfusion fMRI

Perfusion fMRI using arterial spin labeling (ASL) (WILLIAMS et al. 1992; DETRE et al. 1995; KWONG et al. 1995; KIM 1995; WONG et al. 1997) is a useful adjunct to conventional BOLD contrast because it provides potentially better spatial localization and absolute quantitation of CBF, but has less sensitivity than BOLD contrast (see Chap. 6, this volume). It is also important for studies of BOLD contrast mechanisms, which involve complex interactions between CBF, $CMRO_2$, and CBV. Techniques for simultaneous acquisition of BOLD and ASL perfusion signals are

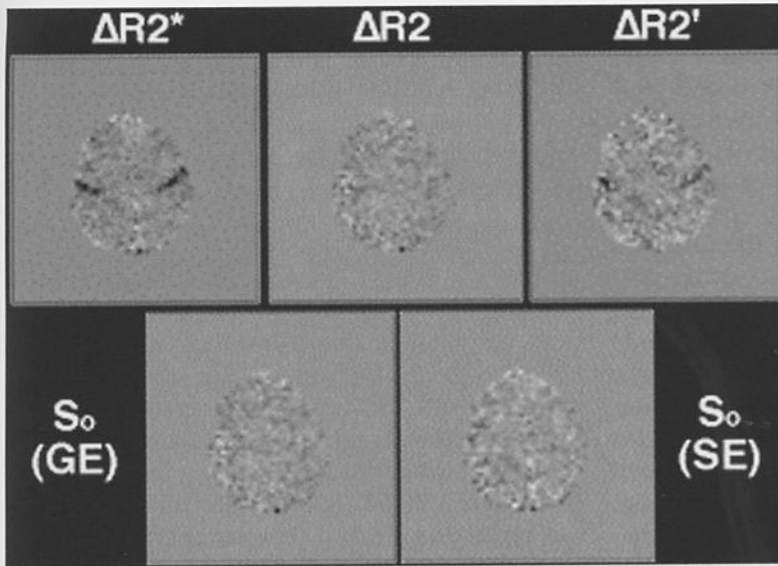


Fig. 17.8. Images of transverse relaxation rate change during bilateral finger tapping. The largest changes are seen in R_2 and almost no change is seen in S_0 .

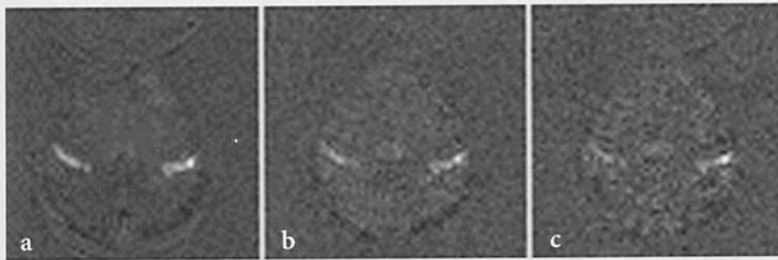


Fig. 17.9a-c. Functional images obtained from a single triple-echo time series. a gradient-recalled echo (GRE; TE=27.1 ms). b Asymmetric spin-echo (ASE); spin-echo occurs at 109.6 ms ($t=-27.1$ ms). c ASE ($t=+27.1$ ms)

described below, along with a discussion of the quality of separation between BOLD and perfusion information.

17.4.1 Imaging Techniques

For any imaging technique that is T_2 or T_2^* sensitive, there is some degree of inherent BOLD contrast. Likewise, for all but very specifically designed sequences, there is some degree of inflow weighting, positive or negative. In this section we discuss the factors that affect the separability of flow and BOLD signals.

17.4.1.1 Pulsed ASL

In ASL in general, the magnetization of the static tissue in the imaging slices is immaterial, as long as

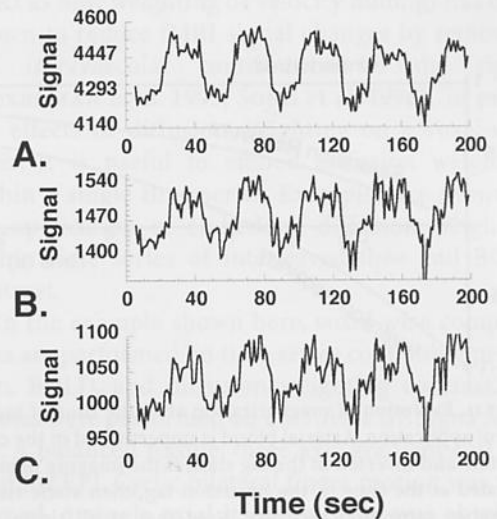


Fig. 17.10A-C. Time course plots from the same motor cortex region as in Fig. 17.9. Plots A, B, C correspond to images A, B, C in Fig. 17.9

it is the same between tag and control conditions (BUXTON et al. 1998). For pulsed ASL, it is relatively straightforward to arrange for the magnetization of the imaging planes to be such that both tag and control images can be used for both the ASL and the BOLD signal. This is done in the following manner (WONG et al. 1997; WONG and BANDETTINI 1996).

The magnetization of the tagged arterial blood follows an inversion recovery curve in the time after the application of the tag, as shown in the bottom curve of Fig. 17.11. In the control state, the arterial magnetization is relaxed, as in the top curve in the figure. If a saturation pulse is applied to the imaging plane immediately prior to the application of the tag pulse, the tissue in the imaging plane undergoes saturation recovery, as in the middle curve of the figure. As usual, the ASL signal is the difference between adjacent tag and control images, irrespective of the static tissue contrast. Under these conditions, the average of adjacent tag/control pairs can be used to construct the BOLD time course. Note that in an average of adjacent images, the time course of the average magnetization of the inflowing arterial blood is the same as the magnetization of the static tissue (i.e., the average of the top and bottom curves in the figure equals the middle curve. Equivalently, the tag condition is negatively flow-weighted (inflow decreases M_z), while the control condition is positively flow-weighted (inflow increases M_z) by the same amount. If the T_1 of arterial blood is identical to that of the static tissue, then these pairwise averaged images are independent of inflow. However, be-

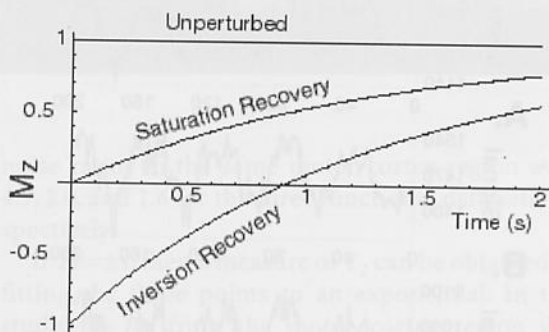


Fig. 17.11. Evolution of magnetization after the time of tag or control application. Arterial blood is unperturbed in the control state and inverted in the tag state. If the imaging plane is saturated at the time of the inversion tag, then static tissue undergoes saturation recovery. Note that at all times, the saturation recovery magnetization equals the average of the unperturbed and the inversion recovery magnetization (see text)

cause the T_1 of blood is slightly different from that of brain tissue, there is a very small amount of flow weighting in the BOLD signal, as estimated below.

17.4.1.2

Continuous ASL

For continuous ASL (WILLIAMS et al. 1992; DETRE et al. 1995), because the inversion of tagged arterial blood is distributed across time, the tagged blood does not follow a simple inversion recovery as in pulsed ASL. For this reason, the scheme outlined above for pulsed ASL does not generate a flow-independent BOLD signal. However, in continuous ASL the control images acquired without perturbation of the inflowing blood are nearly flow independent and can be used as a BOLD time series. There is a very slight positive flow weighting in these images due to the saturation of the imaging slice at the time of image acquisition, and subsequent inflow of relaxed blood, but this effect is small because of the long TR used in continuous ASL.

17.4.2

Separation of BOLD and Perfusion Signals in Pulsed ASL

The raw time course and separated CBF and BOLD components of the signal from a simultaneous pulsed ASL/BOLD finger tapping experiment are shown in Fig. 17.12. In the raw time series, the ASL signal is seen as the rapid image-to-image oscillation, while the BOLD signal is the overall rise and fall of the signal. In the separated time series, the ASL signal is calculated not as a simple pairwise subtraction, but as the difference between each image and the average of the previous and next images. In this manner, the ASL becomes independent of local linear trends in the BOLD signal. Likewise, the BOLD signal is calculated as the average of each image with the average of the previous and next images, providing insensitivity to linear trends in the ASL signal. The residual cross-contamination of the ASL and BOLD signals in the scheme described above is discussed and estimated below.

17.4.2.1

Contamination of the BOLD Signal by Perfusion

Because the T_1 of blood is known to be longer than that of tissue, there is some residual negative flow weighting in the average of tag and control images

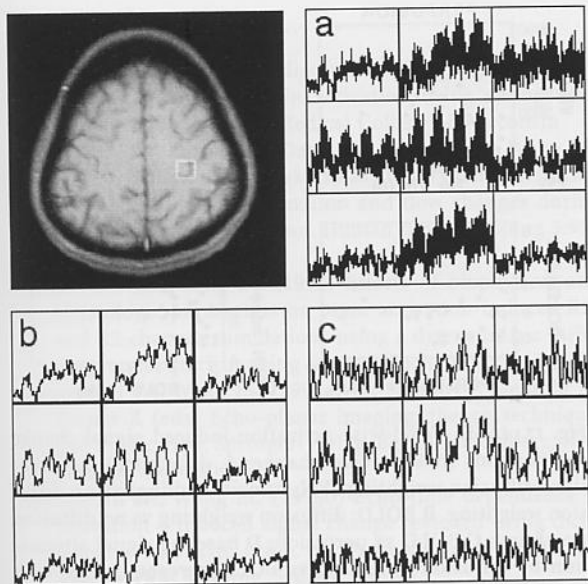


Fig. 17.12a-c. Separation of arterial spin labeling (ASL) and blood oxygen level-dependent (BOLD) components from a raw time series in a combined ASL/BOLD experiment. a Raw time series from each of nine pixels shown in the boxed area of the image. b BOLD time series; c ASL time series (see text)

due to exchange of blood water with tissue water. This residual flow contribution can be estimated by calculating the difference between the magnetization of the tissue compartment in the presence and absence of inflow for a saturation recovery experiment. Using the kinetic inflow model for the ASL signal, in a QUIPSS II experiment with $T_{11}=700$ ms, $T_{12}=1400$ ms, if the transit delay is 1000 ms, the T_1 of blood is 1300 ms, and the T_1 of tissue is 900 ms, the residual flow signal in the average of tag and control images is approximately 18% of the flow signal in the difference signal between tag and control states. This flow contribution has the opposite sign as that of the BOLD signal and thus can only cause underestimation of the BOLD signal.

17.4.2.2

Contamination of the ASL Signal by BOLD

BOLD effects can also contaminate perfusion measurements, but this effect is probably even smaller than the effect of flow on the BOLD signal. To a first approximation, the BOLD effect causes a simple scaling of the MR signal on the order of 2%–4% during activation. If this scaling occurs uniformly throughout the tissue, then this would result in a simple scaling of the flow difference signal. A typical value for the signal-to-noise ratio of the flow mea-

surements is approximately 20 for 3 min of averaging, so changes on the order of 2%–4% would be at the limit of detectability. Furthermore, functional changes in the flow signal are typically on the order of 50% of the flow signal, and would dominate BOLD-related changes. However, the distributions of tissue that give rise to the flow and BOLD signals are different and may result in a more complex interaction between the flow and BOLD signals. The flow signal arises mostly from small arteries, capillaries, and brain parenchyma. The BOLD signal is primarily from veins and tissue surrounding veins and cannot arise from the arterial side of the circulation because arterial oxygenation is essentially constant. The only overlap between the populations of tissues that give rise to flow and BOLD signals is in brain parenchyma surrounding veins. These extravascular tissues are responsible for only about one third of the BOLD signal, as determined by diffusion-weighted BOLD studies (BOXERMAN et al. 1995, SONG et al. 1996;), and thus produce signal changes that are on the order of 1%. If the BOLD signal only increases the brain tissue signal by 1%, then the tissue component of the ASL signal will be increased by 1%, generating errors in the flow measurement that are typically well within the experimental error.

17.5

Embedded Diffusion Weighting

Diffusion weighting (also known in the context of fMRI as flow weighting or velocity nulling) has been shown to reduce fMRI signal changes by removing the intravascular contribution to the signal (BOXERMAN et al. 1995; SONG et al. 1996). To probe the effects of diffusion weighting on a voxel-wise basis, it is useful to embed diffusion weighting within a single time series. Examples are shown of the application of embedded diffusion weighting within time series of interleaved flow and BOLD contrast.

In the example shown here, voxel-wise comparisons are performed on time series containing perfusion, BOLD, and diffusion weighting contrast. All studies were performed on a 1.5 Tesla GE Signa scanner. A balanced torque, three axis gradient coil was used for EPI. Cyclic bilateral finger motion was performed. A single axial imaging plane was obtained using T2*-weighted PICORE (WONG et al. 1997). Selective and nonselective off-resonance inversion was applied for every other image. Diffusion weighting

gradients ($b=10 \text{ s}^2/\text{mm}$) were applied for every other pair of images. The in-plane voxel dimension= $3.8+3.8 \text{ mm}$, slice thickness= 10 mm , $\text{TE}=40 \text{ ms}$, $\text{TR}=2 \text{ s}$, $\text{TI}=1.2 \text{ s}$. A total of 1792 sequential images were obtained, producing four embedded time series of 448 images. Motion correction was performed.

Figure 17.13 shows the anatomical and corresponding functional images created from the four time series. Figure 17.14 shows scatter plots comparing the relative activation induced signal changes ($\Delta\%$ =percent change, Δ =difference). Two main points can be made: (1) The regions of activation between perfusion and BOLD contrast differ (in Fig. 17.13, compare B,C to D,E). Correspondingly, a small inverse relationship exists between perfusion and BOLD signal change magnitudes (Fig. 17.14 C). Generally, regions of highest perfusion changes correspond to BOLD changes of only about 1%. (2) Dif-

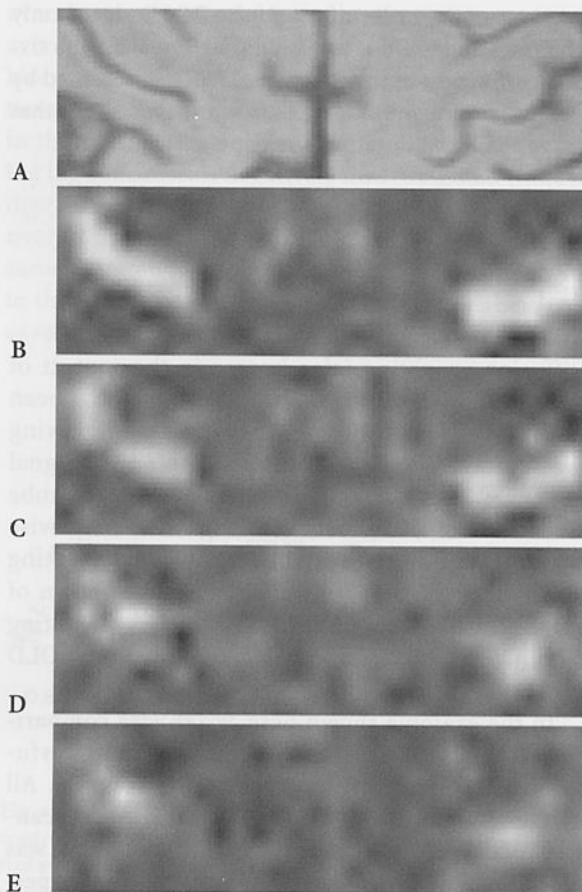


Fig. 17.13. A Anatomical image. The following images are obtained using B BOLD and no diffusion weighting; C BOLD and diffusion weighting; D perfusion and no diffusion weighting; E perfusion and diffusion weighting

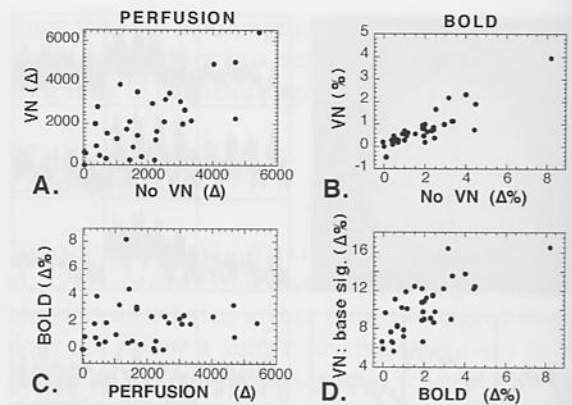


Fig. 17.14A-D. Voxel-wise activation-induced signal change comparisons ($\Delta\%$, percent change; Δ , difference). A Perfusion: diffusion weighting (VN; velocity nulling) vs no diffusion weighting. B BOLD: diffusion weighting vs no diffusion weighting; C BOLD vs perfusion; D baseline signal attenuation by diffusion weighting vs BOLD percent change with activation

fusion weighting, while reducing the BOLD fractional signal change (by about one half, as shown in Fig. 17.14B), does not change the location of activation (in Fig. 17.13, compare B to C). Because of extravascular susceptibility effects, the relative signal change magnitudes are still strongly weighted by blood volume, even though the blood signal itself is destroyed by diffusion weighting. Figure 17.14D also demonstrates this by showing that the largest attenuation of baseline signal by diffusion weighting (corresponding to voxels with high blood volume) corresponds to the largest fractional signal change. This largest fractional signal change remains the largest even with diffusion weighting (Fig. 17.14B).

17.6 Conclusions

Embedded contrast is a simple solution to the need for comparisons of different contrast weightings that require a high degree of temporal and spatial registration. These types of comparisons have proven extremely useful for the study of fMRI contrast mechanisms. In this chapter, methods for embedding several types of contrast were discussed. These included combinations of inflow, T_2 , T_2^* , and T_2' forms of BOLD contrast, and diffusion weighting.

References

- Bandettini PA (1995) PhD dissertation: Magnetic resonance imaging of human brain activation using endogenous susceptibility contrast, Medical College of Wisconsin
- Bandettini PA, Kwong KK, Davis TL, Tootell RBH, Wong EC, Fox PT, Belliveau JW, Weiskoff RM (1997) Characterization of cerebral blood oxygenation and flow changes during prolonged brain activation. *Human Brain Mapping* 5:93-109
- Bandettini PA, Wong EC (1995) Effects of biophysical and physiologic parameters on brain activation-induced R2* and R2 changes: simulations using a deterministic diffusion model. *Int J Imaging Systems Technology* 6:134-152
- Bandettini PA, Wong EC (1998a) In: Schmitt F, Stehling M, Turner R (eds) *Echo-planar imaging: theory, technique, and application*. Springer-Verlag, Berlin, Heidelberg, New York, pp 493-530
- Bandettini PA, Wong EC (1998b) Echo time dependence of activation - induced signal change revisited using diced k-space (DK) acquisition. In: *Proceedings of the 6th Annual ISMRM Meeting, Sydney*, p. 1396
- Bandettini PA, Wong EC, Cox RW, Jesmanowicz A, Hinks RS, Hyde JS (1994) Simultaneous assessment of blood oxygenation and flow contributions to activation induced signal changes in the human brain. In: *Proceedings of the 2nd Annual SMR Meeting, San Francisco*, p. 621
- Bandettini PA, Wong EC, Hinks RS, Tikofsky RS, Hyde JS (1992) Time course EPI of human brain function during task activation. *Magn Reson Med* 25:390-397
- Bandettini PA, Wong EC, Jesmanowicz A; Hinks RS, Hyde JS (1993) Simultaneous mapping of activation - induced $\Delta R2^*$ and $\Delta R2$ in the human brain using a combined gradient-echo and spin-echo EPI pulse sequence. In: *Proceedings of the 12th Annual SMRM Meeting, New York*
- Belliveau JW, Kennedy DN, McKinstry RC, Buchbinder BR, Weiskoff RM, Cohen MS, Vevea JM, Brady TJ, Rosen BR (1991) Functional mapping of the human visual cortex by magnetic resonance imaging. *Science* 254:716-719
- Birn RM, Bandettini PA, Jesmanowicz A, Cox RW (1997a) Bz-Changes in the brain due to speaking and swallowing. In: *Proceedings of the 5th Annual Meeting ISMRM, Vancouver*, p. 458
- Birn RM, Jesmanowicz A, Cox RW (1997b) Correction of dynamic Bz-field artifacts in EPI. In: *Proceedings of the 5th Annual Meeting ISMRM, Vancouver*, p. 349
- Boxerman JL, Bandettini PA, Kwong KK, Baker JR, Davis TL, Rosen BR, Weiskoff RM (1995) The intravascular contribution to fMRI signal change: Monte Carlo modeling and diffusion-weighted studies in vivo. *Magn Reson Med* 34:4-10
- Buxton RB, Frank LR, Wong EC, Siewert B, Warach S, Edelman RR (1998) A general kinetic model for quantitative perfusion imaging with arterial spin labeling. *Magn Reson Med* 40:383-396
- Detre JA, Williams DS, Zhang W, Roberts DA, Leigh JS, Koretsky AP (1995) In: LeBihan D (ed) *Diffusion and perfusion: magnetic resonance imaging*. Raven, New York, pp 269-305
- Davis TL, Kwong KK, Weiskoff RM, Rosen BR (1998) Calibrated functional MRI: mapping the dynamics of oxidative metabolism. *Proc Natl Acad Sci USA* 95:1834-1839
- Frahm J, Bruhn H, Merboldt KD, Hancicke W, Math D (1992) Dynamic MR imaging of human brain oxygenation during rest and photic stimulation. *J Magn Reson Imaging* 2:501-505
- Glover GH, Lemieux SK, Drangova M, Pauly JM (1996) Decomposition of inflow and blood oxygen level-dependent (BOLD) effects with dual-echo spiral gradient-recalled echo (GRE) fMRI. *Magn Reson Med* 35:299-308
- Haacke EM, Al S, Reichenbach JR, Kuppusamy K, Hoogenraad FGC, Takeichi H, Lin W (1997) In vivo measurement of blood oxygen saturation using magnetic resonance imaging: a direct validation of the blood oxygen level-dependent concept in functional brain imaging. *Human Brain Mapping* 5:341-346
- Hennig J, Ernst T, Speck O, Deuschl G, Feifel E (1994) Detection of brain activation using oxygenation sensitive functional spectroscopy. *Magn Reson Med* 31:85-90
- Hennig J, Janz C, Speck O, Ernst T (1995) Functional spectroscopy of brain activation following a single light pulse: examinations of the mechanism of the fast initial response. *Int J Imaging Sys Technol* 6: 203-208
- Kennan RP, Zhong J, Gore JC (1994) Intravascular susceptibility contrast mechanisms in tissues. *Magn Reson Med* 31:9-21
- Kim S-G (1995) Quantification of relative cerebral blood flow change by flow-sensitive alternating inversion recovery (FAIR) technique: application to functional mapping. *Magn Reson Med* 34:293-301
- Kim S-G, Ugurbil K (1997) Comparison of blood oxygenation and cerebral blood flow effects in fMRI: estimation of relative oxygen consumption change. *Magn Reson Med* 38:59-65
- Kwong KK, Belliveau JW, Chesler DA, Goldberg IE, Weiskoff RM, Poncelet BP, Kennedy DN, Hoppel BE, Cohen MS, Turner R, Cheng HM, Brady TJ, Rosen BR (1992) Dynamic magnetic resonance imaging of human brain activity during primary sensory stimulation. *Proc Natl Acad Sci USA* 89:5675-5679
- Kwong KK, Chesler DA, Weiskoff RM, Donahue KM, Davis TL, Ostergaard L, Campbell TA, Rosen BR (1995) MR perfusion studies with T1-weighted echo planar imaging. *Magn Reson Med* 34:878-887
- Menon RS, Ogawa S, Tank DW, Ugurbil K (1993) 4 tesla gradient recalled echo characteristics of photic stimulation-induced signal changes in the human primary visual cortex. *Magn Reson Med* 30:380-386
- Moonen CTW, van Zijl PCM, Frank JA, LeBihan D, Becker ED (1990) Functional magnetic resonance imaging in medicine and physiology. *Science* 250:53-61
- Ogawa S, Lee TM (1992) Functional brain imaging with physiologically sensitive image signals. *J Magn Reson Imaging* 2(P)-WIP (supplement): S22 (Abstract)
- Ogawa S, Lee TM, Kay AR, Tank DW (1990) Brain magnetic resonance imaging with contrast dependent on blood oxygenation. *Proc Natl Acad Sci USA* 87:9868-9872
- Ogawa S, Menon RS, Tank DW, Kim S-G, Merkle H, Ellerman JM, Ugurbil K (1993) Functional brain mapping by blood oxygenation level-dependent contrast magnetic resonance imaging: a comparison of signal characteristics with a biophysical model. *Biophys J* 64:803-812
- Posse S, Olthoff U, Weckesser M, Jancke L, Muller-Gartner HW, Dager SR (1997) Regional dynamic signal changes during controlled hyperventilation assessed with blood

- oxygen level-dependent functional MR imaging. *AJNR* 18:1763-1770
- Posse S, Tedeschi G, Risinger R, Ogg R, LeBihan D (1995) High speed 1H spectroscopic imaging in human brain by echo planar spatial-spectral encoding. *Magn Reson Med* 33:34-40
- Prinster A, Pierpaoli C, Turner R, Jezzard P (1997) Simultaneous measurement of ΔR_2 and ΔR_2^* in cat brain during hypoxia and hypercapnia. *NeuroImage* 6:191-200
- Rosen BR, Belliveau JW, Chien D (1989) Perfusion imaging by nuclear magnetic resonance. *Magn Reson Q* 5:263-281
- Song AW, Wong EC, Tan SG, Hyde JS (1996) Diffusion weighted fMRI at 1.5 T. *Magn Reson Med* 35:155-158
- Turner R, LeBihan D, Moonen CTW, Despres D, Frank J (1991) Echo-planar time course MRI of cat brain oxygenation changes. *Magn Reson Med* 22:159-166
- van Zijl PCM, Eleff SM, Ulatowski JA, Oja JME, Ulug AM, Traystman RJ, Kauppinen RA (1998) Quantitative assessment of blood flow, blood volume, and blood oxygenation effects in functional magnetic resonance imaging. *Nature Med* 4:159-167
- Weiskoff RM, Zuo CS, Boxerman JL, Rosen BR (1994) Microscopic susceptibility variation and transverse relaxation: theory and experiment. *Magn Reson Med* 31:601-610
- Williams DS, Detre JA, Leigh JS, Koretsky AP (1992) Magnetic resonance imaging of perfusion using spin-inversion of arterial water. *Proc Natl Acad Sci USA* 89:212-216
- Wong EC, Bandettini PA (1996) Two embedded techniques for simultaneous acquisition of flow and BOLD signals in functional MRI. In: Fourth Meeting, International Society for Magnetic Resonance in Medicine, New York, p. 1816
- Wong EC, Buxton RB, Frank LR (1997) Implementation of quantitative perfusion imaging techniques for functional brain mapping using pulsed arterial spin labeling. *NMR Biomed* 10:237-249